

Modeling sound transmission through apertures with diffraction

U. Peter Svensson¹

Acoustics group, Dept. of electronic systems, Norwegian University of Science and Technology NO-7491 Trondheim, Norway

Shahin Sohrabi²

Laboratori d'Enginyeria Acústica i Mecànica (LEAM),Universitat Politècnica de Catalunya C/Colom 11, 08222 Terrassa, Spain

ABSTRACT

Sound transmission through an aperture in a thin wall is a classical scattering problem with various applications in building acoustics. In particular, the use of active noise control for open windows can be viewed as an aperture scattering problem. Diffraction-based modeling of scattering is very efficient and accurate for convex scattering objects but has been shown to be less accurate for the transmission through circular apertures, at low frequencies. In this study we investigate the accuracy of edge-diffraction based modeling of sound transmission through circular and square apertures. Reference solutions are computed with a boundary element formulation for this case. Results confirm that the diffraction modeling gives accurate results for mid-to-high frequencies. For low frequencies and skewed transmission angles, the diffraction-based method gives larger errors.

1. INTRODUCTION

The computation of scattering by rigid polyhedra can be done efficiently and accurately by the edge source integral equation, ESIE, method, [1]. The ESIE method has been compared with reference calculations with the boundary element method and was shown to give very similar results for the scattering by a cube [2].

For non-convex scattering objects, however, the ESIE method is less accurate, as shown in [3] for the case of a circular aperture in a thin wall. This special case of non-convex scattering geometry was further investigated in [4], and it was shown that the lack of so-called slope diffraction in the ESIE modeling explains the lack of accuracy. To be precise, the ESIE method computes second- and higher-order diffraction whereas first-order diffraction is computed by the method presented in [5]. An aperture in a thin wall gives rise to first-order diffraction, according to the underlying secondary source, or edge source, model [6]. According to the ESIE method, second-order diffraction, on the other hand, gets zero amplitude for an aperture in a thin baffle, and as a consequence also higher-order diffraction gets zero amplitude.

¹peter.svensson@ntnu.no

²shahin.sohrabi@upc.edu

Summers showed that the secondary source method underestimates the sound power transmission coefficient by 2.1 dB for very low frequencies for a circular aperture [3]. No further values were presented by Summers, so the topic of this paper is to quantify further the difference between the edge source model and a reference solution. The latter is computed by a boundary element method which is formulated for the special case of an aperture in a thin wall. Parts of this work were presented in [7].

This idealized special case is straightforward to study with numerical methods, but nevertheless has practical relevance. The sound transmission through an open window, and through other openings between spaces, can often be studied using a thin-wall assumption as a first model. Expanding the study to apertures in thick walls is an important step in future studies.

2. THEORY AND METHODS

2.1. Bouwkamp's low-frequency expressions, and an integral equation formulation

The wave transmission through an aperture in a thin rigid baffle is a classical case in both acoustics and electromagnetics. The work by Bouwkamp serves as an early reference, with a large number of references to other work [8]. The problem has been studied more recently as well [9], [10], [11] and low-frequency asymptotic expressions have been derived for circular and elliptic apertures in these studies, also for non-perpendicular incidence. As one example, the transmitted sound pressure amplitude, $p_{\text{trans}}(\omega, \theta)$, in the far-field, at distance r, for a perpendicularly incident plane wave of amplitude p_{in} towards a circular aperture of radius a in a rigid baffle is given by Bouwkamp as a low-frequency (LF) asymptotic expression,

$$p_{\text{trans,LF}}(\omega,\theta) = \frac{2a}{\pi} \frac{e^{-jkr}}{r} \left[1 + \left(\frac{1}{3} - \frac{4}{\pi^2} - \frac{1}{6}\sin\theta \right) (ka)^2 + O\left((ka)^4\right) \right]$$
(1)

where $k = \omega/c$, c being the speed of sound, and a time-harmonic factor $e^{j\omega t}$ is assumed. The angle θ is the angle with respect to the symmetry axis of the circular aperture, see Figure 1. Bouwkamp also gave asymptotic expressions for the power transmission factor, τ (which was found by integrating the expression for p^2 , based on Equation 1, over θ), for the rigid baffle, as

$$\tau_{\rm LF} = \frac{8}{\pi^2} \left[1 + \left(\frac{4}{9} - \frac{4}{\pi^2} \right) (ka)^2 + O\left((ka)^4 \right) \right] \tag{2}$$

In addition to asymptotic solutions for a circular aperture, Bouwkamp gave an integral equation formulation for the field in the aperture, which can be used for numerical solutions for arbitrarily shaped apertures. One can also arrive at the integral equation from using the Rayleigh integral, which gives the sound pressure in a point \mathbf{x} , behind (that is, on the opposite side of the baffle, seen from the side of the incident sound wave) the thin rigid baffle, as an integral over the aperture A, and the evaluation of the surface integral requires knowledge of the normal particle velocity, u_n , at the points \mathbf{x}_A in the aperture,

$$p(\mathbf{x},\omega) = \frac{\mathrm{j}\omega\rho_0}{2\pi} \int_A u_n(\mathbf{x}_A,\omega) \frac{\mathrm{e}^{-\mathrm{j}kr}}{r} dA$$
 (3)

where $r = |\mathbf{x} - \mathbf{x}_A|$. Now, if the receiver point \mathbf{x} is placed in the plane of the baffle, inside the aperture, an integral equation results when we view $u_n(\mathbf{x}_A)$ as an unknown function, and use the fact that $p(\mathbf{x}_A, \omega)$ is known: the sound pressure in the aperture is identical with the incident free-field sound pressure [9]. Then

$$p(\mathbf{x}_A, \omega) = p_{\text{in}}(\mathbf{x}_A, \omega) = \frac{j\omega\rho_0}{2\pi} \int_A u_n(\mathbf{x}_A', \omega) \frac{e^{-jkr}}{r} dA$$
 (4)

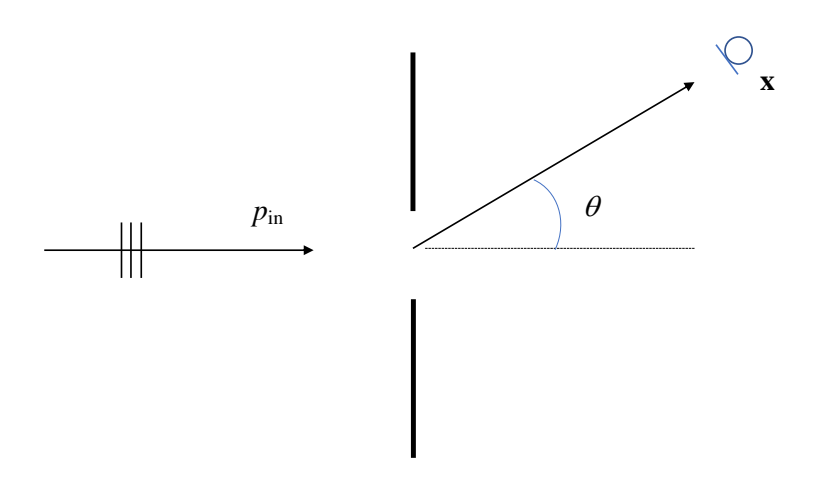


Figure 1: Illustration of a circular aperture in a baffle, drawn with a thick line. A plane wave with normal incident hits the aperture from the left. A receiver, at \mathbf{x} , is positioned at an angle θ with respect to the aperture symmetry axis, shown with a dashed line.

Solving this integral equation numerically becomes a form of boundary element method, and the numerical approach chosen in this study is described in the next section. It can be noted that Equation 4 can be computed for near- and far-field receiver positions.

2.2. Numerical solution of Equation 4 - a Boundary Element Method

A simple approach is used here, subdividing the aperture into elements across which a constant particle velocity is assumed. It is known that the particle velocity, or sound pressure gradient, becomes singular as one moves closer to the edge of the aperture, and therefore, this simple approach converges slowly. It will be shown, however, that adequate accuracy results in our study of square and circular apertures. The square apertures are subdivided into equally sized elements whereas the circular aperture is subdivided into annular rings of equal widths. Equation 4 then becomes a sum, so that the sound pressure at a discrete point $\mathbf{x}_{A,i}$ is a sum of the contributions from the N elements,

$$p_{\text{in}}(\mathbf{x}_{A,i},\omega) = \frac{\mathrm{j}\omega\rho_0}{2\pi} \sum_{j=1}^{N} \int_{A_j} u_n(\mathbf{x}_A',\omega) \frac{\mathrm{e}^{-\mathrm{j}kr}}{r} dA \tag{5}$$

where the integration is over each little element A_j . This discretization leads to N equations which can be gathered in a matrix equation,

$$\mathbf{Z}\mathbf{U} = \mathbf{P}_{in} \tag{6}$$

where **U** is vertical array, size (N, 1) of the unknown particle velocities (assumed constant across each element) and \mathbf{P}_{in} is also a vertical array, size (N, 1), of the known incident sound pressures at the center points of each element. The matrix **Z**, of size (N, N), contains cross-impedance terms, where term $Z_{i,j}$ in row i and column j gives the sound pressure at the center of element i, for a unit vibration velocity of element j:

$$Z_{i,j} = \frac{j\omega\rho_0}{2\pi} \int_{A_i} \frac{e^{-jkr}}{r} dA \tag{7}$$

Computing the integral for this Z-term is the same as calculating the sound pressure from a piston. Importantly, the "self-term", when j = i, which has a singularity due to the fact that $r \to 0$ inside the element, is easily computed to high accuracy with standard methods for the radiation from pistons, either as frequency-domain or time-domain expressions [12]. If a square aperture is subdivided into equally sized square elements, then many $Z_{i,j}$ will be identical.

2.3. Edge diffraction Method

The edge diffraction method decomposes the sound pressure into a sum of four terms, whether one uses a time-domain or frequency-domain description,

$$p(\mathbf{x}) = p_{\text{direct}}(\mathbf{x}) + p_{\text{specular}}(\mathbf{x}) + p_{\text{diff. 1}}(\mathbf{x}) + p_{\text{higher-order diff.}}(\mathbf{x})$$
(8)

where $p_{\rm direct}$ is the same as the free-field incident field *if the receiver can see the source*, and zero otherwise. Thus, behind the baffle, the direct sound will be non-zero in a narrow duct created by the source and the aperture. The term $p_{\rm specular}$ represents the specular reflection according to geometrical acoustics principles, and this term will be non-zero only on the source side of the baffle. The first-order diffraction term, $p_{\rm diff.\,1}$, is generated by the edge of the aperture and reaches all possible receiver points, because a first-order diffraction wave is generated by all points of an edge which can see the source and the receiver, [6], [5]. The last term, $p_{\rm higher-order\,diff.}$, is generated as waves from the source, to one point along an edge, via another point along an edge, repeated a number of times, and then to the receiver. For this special case of an aperture in a rigid, thin wall, the analytic edge source directivity functions have the amplitude zero for a wave from one edge point to another edge point. Therefore, second- and higher-order diffraction is zero for this case [4].

As a consequence of the lack of higher-order diffraction for the aperture in the thin wall, in this study it suffices to compute the first three terms in Equation 8. The first-order diffraction is computed as a integral along the aperture edge, and the integral involves directional edge sources. For the special case of a thin edge and normal incidence, the directivity function gets simplified, and the integral takes the form [6], [5],

$$p_{\text{diff. 1}}(\mathbf{x}) = -\frac{1}{8\pi} \int_{\Gamma} \beta \frac{e^{-jk(m+l)}}{ml} ds_{\Gamma}$$
(9)

where Γ represents the aperture edge, s_{Γ} is the position along the edge, m is the distance from the source point to the edge point, l is the distance form the edge point to the receiver, and β is the directivity function, which has the form

$$\beta = 2 \cosh \frac{\eta}{2} \left[\frac{\cos(\frac{\pi}{4} + \frac{\theta_{R}}{2})}{\cosh^{2} \frac{\eta}{2} - \sin^{2}(\frac{\pi}{4} + \frac{\theta_{R}}{2})} + \frac{\cos(\frac{\pi}{4} - \frac{\theta_{R}}{2})}{\cosh^{2} \frac{\eta}{2} - \sin^{2}(\frac{\pi}{4} - \frac{\theta_{R}}{2})} \right]$$

where

$$\cosh \frac{\eta}{2} = \frac{\cos \frac{\varphi_{S} - \varphi_{R}}{2}}{\sqrt{\sin \varphi_{S} \cdot \sin \varphi_{R}}}$$

The geometrical parameters are illustrated in Figure 2, which shows that the angles are based on the aperture edge tangent line, and the source and receiver planes, which involve the edge tangent line, and the source, or receiver, respectively. For the normal plane wave incidence a further simplication results, because the angle $\varphi_S = \pi/2$ and then

$$\cosh \frac{\eta}{2} = \frac{1}{\sqrt{\sqrt{2}}} \frac{\cos \frac{\varphi_R}{2} + \sin \frac{\varphi_R}{2}}{\sqrt{\sin \varphi_R}}$$

The *Edge diffraction Matlab toolbox*, freely available on Github, [13], computes the terms in Equation 9, but only for convex scattering objects. A small modification was made of the code so that the first three terms were computed also for apertures in thin baffles (which are non-convex geometries, when viewed as scattering objects). The receiver positions were either in the far-field, as described further below, or in the aperture itself. For the latter, it is not the sound pressure but the particle velocity which is the desired quantity to compute. The details are not presented here, but a similar derivation of the gradient of the sound pressure, in the plane of a thin sheet, was presented in [14]. For these calculations a separate Matlab was implementation was made, using Matlab's built-in numerical integration functions.

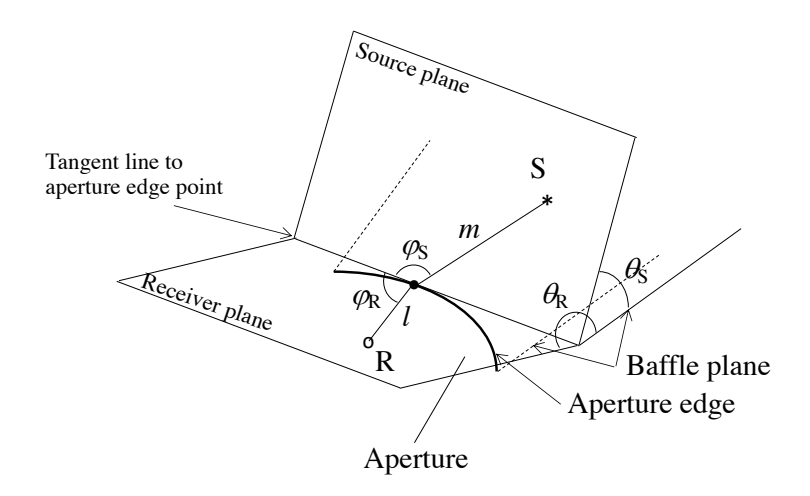


Figure 2: Illustration of a part of an aperture edge in a baffle. For each point of the aperture edge, a tangent line exists. This tangent line forms a "source plane" together with the source position, and a "receiver plane" together with the receiver position. These planes are used to define the angles θ_S , θ_R , φ_S , and φ_R .

2.4. Computing the power transmission factor

The power transmission factor can be computed in two different ways, based on the far-field or the near-field of the transmitted field. In both cases the incident power is the same,

$$W_{\rm in} = I_{\rm in} A_{\rm aperture} = \frac{p_{\rm in,rms}^2}{\rho_0 c} A_{\rm aperture}$$

1. A number of receiver positions can be distributed over a hemispherical surface, A_{hemi} , in the far field, with a radius r_{far} . Thus,

$$W_{\text{transm.}} = \int_{A_{\text{hemi}}} \frac{p_{\text{far-field,rms}}^2}{\rho_0 c} dS = \frac{2\pi r_{\text{far}}^2}{\rho_0 c} \text{Mean} \left[p_{\text{far-field,rms}}^2 \right]$$

$$\tau_{\text{far-field}} = \frac{W_{\text{transm.}}}{W_{\text{in}}} = \frac{2\pi r_{\text{far}}^2}{p_{\text{in rms}}^2 A_{\text{aperture}}} \text{Mean} \left[p_{\text{far-field,rms}}^2 \right]$$
(10)

2. The transmitted intensity, $I_{\text{transm.}} = \frac{1}{2} \text{Re} [p \cdot u_n]$, can be computed across the aperture and the integration of the intensity can give the transmitted power. It can be noted that the sound pressure is known and equal to the free-field incident sound pressure. Furthermore, for normal plane wave incidence, the incident sound pressure is constant across the aperture, and then

$$\tau_{\text{near-field}} = \frac{W_{\text{transm.}}}{W_{\text{in}}} = \frac{\int_{A_{\text{aperture}}} I_{\text{transm.}} dA}{W_{\text{in}}} = \frac{\frac{1}{2} p_{\text{in}} \text{Mean} \left[\text{Re}[u_n] \right]}{p_{\text{in,rms}}^2 / (\rho_0 c)} = \rho_0 c \cdot \text{Mean} \left[\text{Re}[u_n] \right]$$
(11)

These two methods should converge to the same value, as the number of discretization points in the aperture, and the number of receiver points, are increased.

2.5. Richardson extrapolation

An acceleration technique is used here, the so-called Richardson extrapolation. It was explained for similar numerical methods in [2] but can be described briefly as follows. When a discretization scheme is used for the numerical computation of some value, \hat{u}_n , the accuracy will depend on some

kind of step size, or element length, Δ . For many numerical schemes we can, for small Δ , assume that the error follows some polynomial dependence on Δ :

$$\hat{u}_n = u_{n,\text{true}} + E_1 \Delta^1 + E_2 \Delta^2 + O\left(\Delta^3\right) \tag{12}$$

where the leading term can be Δ , or Δ^2 , etc, depending on the numerical scheme. As an example let's assume that we know that the calculation of \hat{u}_n has an error that goes as $O(\Delta)$, but we don't know the value of E_1 and we don't know $u_{n,\text{true}}$. We can rewrite Equation 12 as

$$\hat{u}_n = u_n' + E_1 \Delta^1 \tag{13}$$

where

$$u'_n = u_{n,\text{true}} + O\left(\Delta^2\right) \tag{14}$$

Then we can compute \hat{u}_n for two different values of Δ , and Equation 13 gives us two equations and two unknowns, so we find an *improved* estimate u'_n , the error of which goes as $O(\Delta^2)$ see Equation 14 rather than our directly computed values \hat{u}_n , which have $O(\Delta)$. If one doesn't know the leading exponent for the numerical method at hand, it can be found empirically from a set of calculations [2].

For the numerical computations that follow, a number of discretizations were used, followed by Richardson extrapolation.

2.6. Studied cases

In this study, we include a circular aperture and a square aperture, for perpendicular (normal) plane wave incidence. For the circular aperture, we subdivide the aperture into N concentric rings, and calculate the cross-impedance terms, given by Equation 7, for the contribution from one piston shaped as an annular ring, to a a receiver point at the center of all the annular ring-shaped elements, see Fig. 4(a). The matrix Equation 6 is then solved to give the particle velocities of the N elements/pistons. Finally, the totally transmitted power is computed as an integral over the intensity in the aperture. The value of the power transmission factor is finally studied as function of number of elements, N, and Richardson extrapolation is applied. When the extrapolation gives stable values, it is assumed that the numerical solution has given an adequately converged value. The particle velocities across the aperture are also computed with the edge diffraction method, described briefly above.

For the square aperture, the elements are also square, and the cross-impedance terms are computed as the sound pressure from a square piston in a baffle, for all the receiver points needed, that is, all the center points of the square elements, see Figure 4(b). The matrix Equation 6 is solved to give the particle velocity values in the aperture. Once these are known, the transmitted sound pressure is computed with Equation 3 for a number of farfield receiver positions. The sound pressure at the far-field receiver positions is also computed with the edge diffraction method, and then the modified version of ED toolbox is used.

3. RESULTS AND DISCUSSION

3.1. A circular aperture

Figure 4 shows results with the BEM approach and circular elements as shown in Figure 3(a). Figure 4(a) shows the particle velocity amplitude as function of radial position inside the aperture. The singular behaviour at the edge can be clearly seen. Also shown is the average value of the real part of the particle velocity amplitude. Apparantly, the particle velocity is dominated by a reactive part for this low frequency. In Figure 4(b), the power transmission factor, τ , as computed from the average of the real part of the particle velocity. Results are shown for 8 different numbers of concentric annular elements, and extrapolated results are shown as well, using the polynomial exponent 1 for the error model. This low exponent is caused by the integral approach which corresponds to a midpoint method.

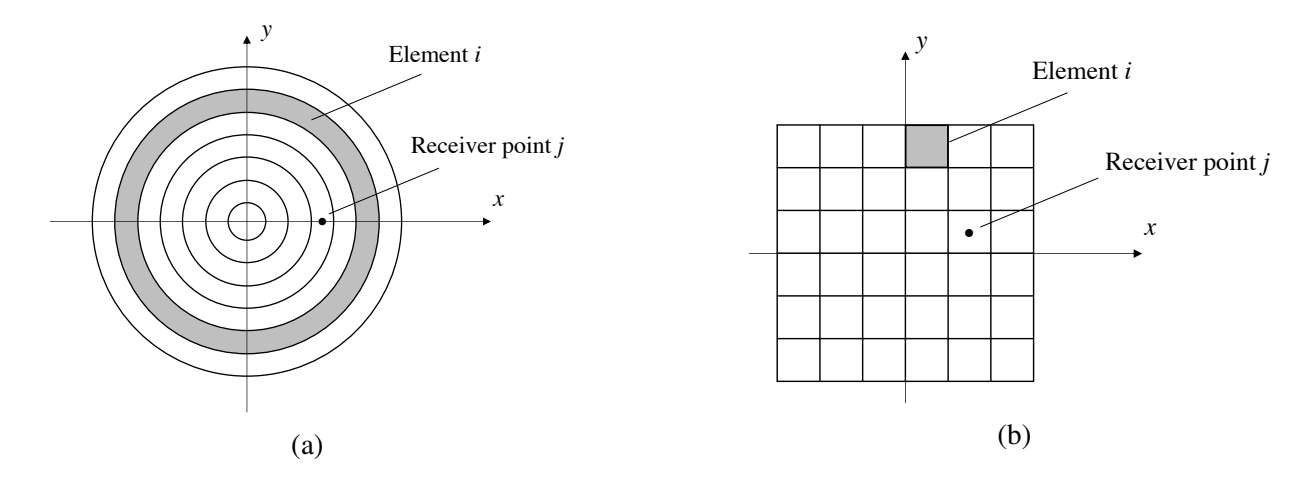
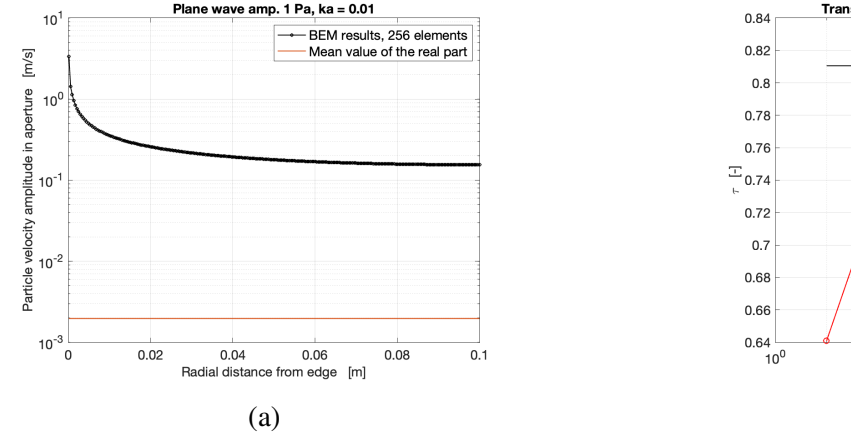


Figure 3: For both (a) the circular, and (b) the square, aperture the cross-impedance term $Z_{i,j}$ gives the sound pressure at receiver point j, at the center of element j, for a unit vibration velocity of element i.

Finally, the reference result according to Equation 2 is also plotted as a constant value. Numerically, the reference result is $\tau_{\rm ref.}=0.8105726$ and the best extrapolated result is $\tau=0.8105753$, which has a relative error of 3.3e-6. The best directly computed value is $\tau=0.8083545$, which has a relative error of 1.4e-3. These results seem to confirm that the simple numerical approach can give adequate accuracy, at least for a circular aperture, and a low frequency. Furthermore, the extrapolation technique also seems to work efficiently for increased precision.

The transmission coefficient was also computed with first-order diffraction, computing the particle velocity in the aperture, at the same element midpoints as was done with the BEM approach, and the results are shown in Figure 5. The results with the diffraction method converge towards the value 0.5, which is -2.1 dB relative to the reference results, and this error was found also by Summers in [3].



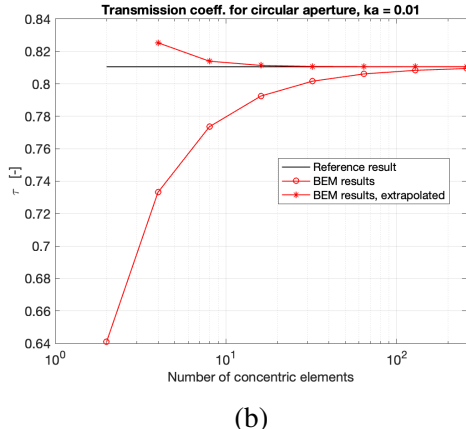


Figure 4: Results for the circular aperture using the BEM approach, for ka=0.01. (a) Particle velocity amplitude in the aperture, computed with 256 concentric elements. Also shown is the mean value of the real part, which gives the transmitted power. Note the logarithmic amplitude scale. (b) The transmission coefficient, τ , calculated from Equation 11, for different number of elements. Also shown are the extrapolated values and the reference solution.

3.2. A square aperture

For the square aperture, the particle velocity in the aperture was computed with the BEM, in the same way as for the circular aperture, but with elements as illustrated in Figure 3(b). In addition, the far-field resuls were computed by distributing 1000 receivers over a hemisphere with a radius of 50 m

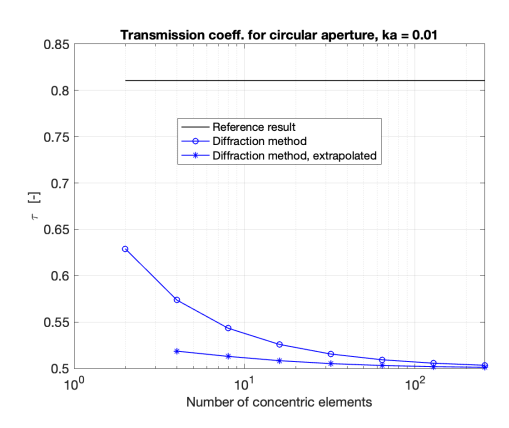


Figure 5: Transmission coefficient, τ , for the circular aperture using the diffraction method, for ka = 0.01, based on the same number of discrete points in the aperture as in Figure 5. Also shown are the extrapolated values and the reference solution. Note the different scale as compared with Figure 4(b).

(the aperture had the size of 1m by 1m), see Figure 6. The far-field results were also computed with the diffraction method.

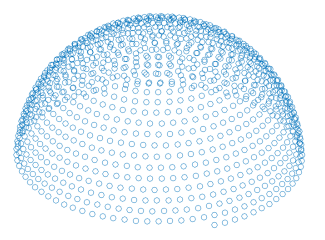
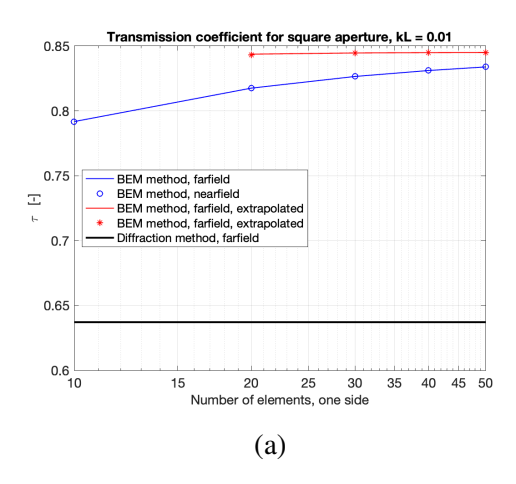


Figure 6: Illustration of 1000 receiver positions that are distributed evenly across a hemispherical surface.

No reference solution is available for the square aperture, but the excellent agreement with the reference result for the circular aperture gives us confidence in our BEM results also for the square aperture. Figure 7(a) shows the results for the BEM approach and the diffraction method, for a low frequency, expressed as kL = 0.01, where L is the sidelength of the square aperture. First, one can observe that for this low frequency, there are extremely small differences between the near-field and far-field results computed with the BEM. This is caused by the omnidirectionality of the radiation for the low frequency studied here. One can also observe that the Richardson extrapolation converges towards a value of 0.8450. The result with the diffraction method gives a value of 0.6372, which is 1.2 dB lower than the BEM result. The low-frequency error with the diffraction method is apparantly a bit smaller for a square aperture than it is for the circular aperture. In Figure 7(b), the real part of the particle velocity in the aperture is shown, for the most accurate BEM calculation, with 50 by 50 elements, plotted with a linear amplitude scale. One can see amplitudes that might be singular towards the four edges of the square aperture, which offers a numerical challenge for the computations.

The transmitted field is analyzed further, for a number of frequencies. Figure 8 shows the far-field sound pressure amplitude as function of radiation angle θ (see Figure 1) for a low and a high frequency, expressed as kL. The two values of kL correspond to 10 Hz and 316 Hz, respectively, for an aperture of size 1m by 1m. It can be observed that somewhat larger errors result for transmission angles larger than 80 degrees. In addition, the diffraction method does not give an omnidirectional



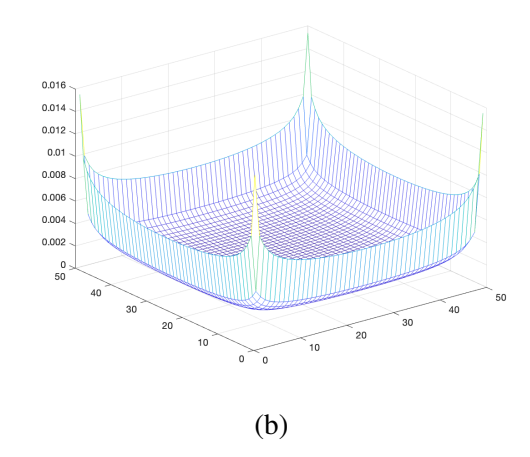


Figure 7: (a) Transmission coefficient, τ , for the square aperture using the BEM and the diffraction method, for kL=0.01. For the BEM the transmitted power is computed both from the intensity in the aperture, as for the circular aperture ("nearfield") and also from far-field receivers ("farfield"). Also shown are the extrapolated values. The results with the diffraction method are only computed as far-field values and are thus independent of the BEM-discretization in the aperture. (b) The real part of the particle velocity in the aperture, for the 50 elements by 50 elements BEM computation.

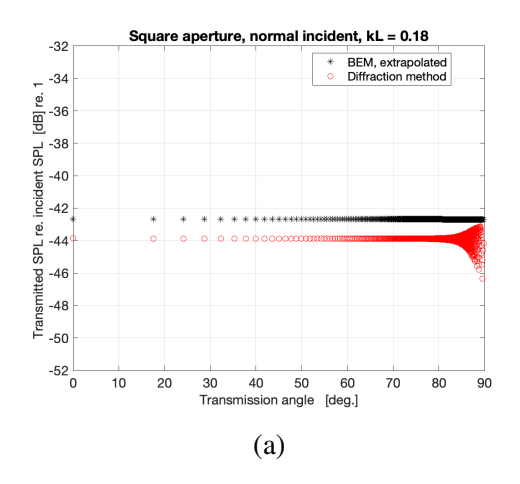
field for the largest transmission angles.

To analyze the error with the diffraction method as function of frequency, we subdivide the results into two angle regions, 0-80 degrees, and 80-90 degrees. Thus, Figure 9 presents the means and percentile values for those two receiver groups, as function of frequency, again expressed as kL. The BEM results are based on calculations with the number of elements being up to 140 by 140 = 19600, which implies that an inversion of a 19600 by 19600 matrix is required for solving Equation 6. Richardson extrapolation was used for all 1000 receiver position sound pressures. It can be observed that for transmission angles smaller than 80 degrees, the mean error is smaller than ±0.5 dB when kL > 1.3, which corresponds to 71 Hz for a 1m by 1m aperture. For transmission angles between 80 and 90 degrees, the mean error is smaller than ± 0.5 dB when kL > 2.8, which corresponds to 160 Hz for a 1m by 1m aperture. The percentile values show that for transmission angles smaller than 80 degrees, 95% of the receiver points have an error within [-1 dB, +0.5 dB] for kL > 0.75, that is, for frequencies above 41 Hz for a 1m by 1m aperture. For transmission angles larger than 80 degrees, the range of errors is substantially larger, and 95% of the receiver points have an error within [-2.5] dB, +1.5 dB] across the entire frequency range. It should be noticed, however, that for very large transmission angles and high frequencies, the transmitted sound is very weak. An indication of this can be seen in Fig. 8(b), where the transmitted sound at 85-90 degrees is around 15 dB weaker than for the main direction of 0 degrees. Therefore, the larger errors (for high frequencies and large transmission angles) have very little influence on the totally transmitted sound field.

Future work should include the study of rectangular apertures, and possibly also other shapes. Furthermore, apertures in thick walls should be addressed.

4. CONCLUSIONS

The sound transmission through a circular and square aperture in a thin wall has been studied using a boundary element method to give reference result, and the edge diffraction method. It was found that the low-frequency asymptoic value of the power transmission coefficient is underestimated by 2.1 dB with the edge diffraction method for the circular aperture, which confirms earlier findings by



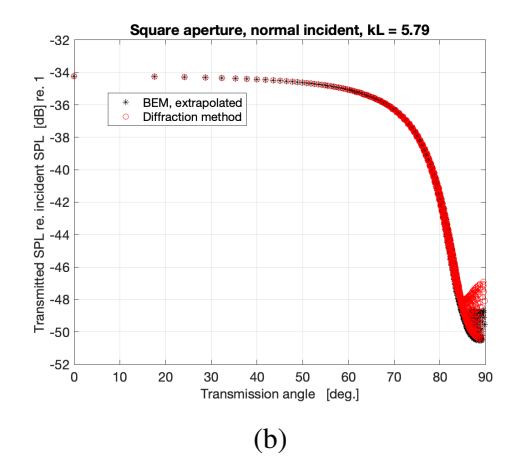


Figure 8: The transmitted sound pressure level (SPL) relative to the incident SPL for a square aperture and (a) a low frequency where the transmitted sound is omnidirectional, and (b) a higher frequency where the transmitted sound is no longer omnidirectional.

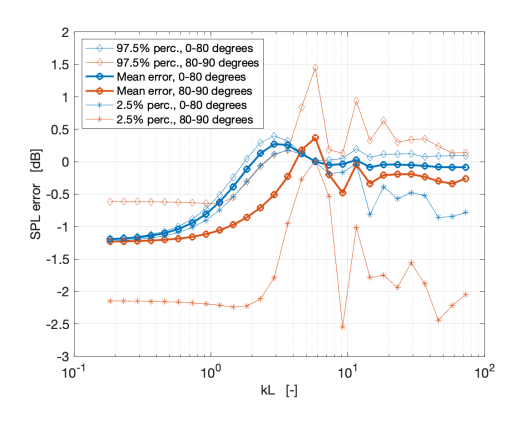


Figure 9: Error for the transmitted SPL, defined as SPL with diffraction method minus SPL with BEM. The mean and percentile values are based on 272 receivers (0-80 degrees) and 728 receivers (80-90 degrees), respectively.

Summers, [3], and by 1.2 dB for the square aperture. For the square aperture, the edge diffraction method gives far-field sound pressure values that for 95% of all receiver points are within [-1 dB,+0.5 dB] of the reference result, for transmission angles smaller than 80 degrees, as long as kL > 0.75 (that is, that one side of the aperture is larger than 1/8th of the wavelength). For transmission angles larger than 80 degrees, 95% of the far-field sound pressure values are predicted within [-2.5 dB,+1.5 dB] with the diffraction method.

REFERENCES

- [1] Andreas Asheim and U. Peter Svensson. An integral equation formulation for the diffraction from convex plates and polyhedra. *The Journal of the Acoustical Society of America*, 133(6):3681–3691, 2013.
- [2] Sara R. Martin, U. Peter Svensson, Jan Slechta, and Julius O. Smith. Modeling sound scattering using a combination of the edge source integral equation and the boundary element method. *The Journal of the Acoustical Society of America*, 144(1):131–141, 2018.
- [3] Jason Summers. Inaccuracy in the treatment of multiple-order diffraction by secondary-edge-source methods (1). *The Journal of the Acoustical Society of America*, 133(6):3673–3676, 2013.

- [4] Sara R. Martin and U. Peter Svensson. Double diffraction models: a study for the case of non-convex bodies. Krakow, Poland, 7-12 Sept. 2014.
- [5] U. Peter Svensson, Paul T. Calamia, and Shinsuke Nakanishi. Frequency-domain edge diffraction for finite and infinite edges. *Acta Acustica united with Acustica*, 95:568–572, 2009.
- [6] U. Peter Svensson, Roger I. Fred, and John Vanderkooy. An analytic secondary source model of edge diffraction impulse responses. *The Journal of the Acoustical Society of America*, 106(5):2331–2344, 1999.
- [7] U. Peter Svensson, Andreas Asheim, and Sara R. Martin. Sound propagation through an aperture with edge diffraction modeling (abstracts). *The Journal of the Acoustical Society of America*, 141(5):3784, 2017.
- [8] C. J. Bouwkamp. Diffraction theory. *Reports on progress in physics*, 17(1):35–100, 1954.
- [9] J. Van Bladel. Low frequency scattering through an aperture in a rigid screen. *Journal of Sound and Vibration*, 6(3):386–395, 1967.
- [10] W. E. Williams. Scattering through apertures in screens. *Journal of Sound and Vibration*, 13(1):37–42, 1970.
- [11] R. de Smedt. Low frequency scattering through an aperture in a rigid screen some numerical results. *Journal of Sound and Vibration*, 75(3):371–386, 1981.
- [12] Gerald R. Harris. Review of transient field theory for a baffled planar piston. *The Journal of the Acoustical Society of America*, 70(1):10–20, 1981.
- [13] U. Peter Svensson. Edge diffraction matlab toolbox.
- [14] David P. Hewett and U. Peter Svensson. The diffracted field and its gradient near the edge of a thin screen (1). *The Journal of the Acoustical Society of America*, 134(6):4303–4306, 2013.